Journal of Medical Robotics Research, Vol. 2, No. 1 (2017) 1750001 (14 pages)

DOI: 10.1142/S2424905X17500015

Journal of Medical Robotics Research
http://www.worldscientific.com/worldscinet/jmrr

Journal of Medical Robotics Research

Toward Transoral Peripheral Lung Access: Combining Continuum Robots and Steerable Needles*

Philip J. Swaney[†,‖], Arthur W. Mahoney[†], Bryan I. Hartley[‡], Andria A. Remirez[†], Erik Lamers[†], Richard H. Feins[§], Ron Alterovitz[¶,**], Robert J. Webster III[†,††]

[†]*Mechanical Engineering, Vanderbilt University, Nashville, TN 37235, USA*

[‡]*Department of Radiology and Radiological Sciences Vanderbilt University, Nashville, TN 37235, USA*

[§]*Division of Cardiothoracic Surgery, University of North Carolina School of Medicine Chapel Hill, NC 27599, USA*

[¶]*Department of Computer Science, University of North Carolina at Chapel Hill Chapel Hill, NC 27599, USA*

Lung cancer is the most deadly form of cancer in part because of the challenges associated with accessing nodules for diagnosis and therapy. Transoral access is preferred to percutaneous access since it has a lower risk of lung collapse, yet many sites are currently unreachable transorally due to limitations with current bronchoscopic instruments. Toward this end, we present a new robotic system for image-guided trans-bronchoscopic lung access. The system uses a bronchoscope to navigate in the airway and bronchial tubes to a site near the desired target, a concentric tube robot to move through the bronchial wall and aim at the target, and a bevel-tip steerable needle with magnetic tracking to maneuver through lung tissue to the target under closed-loop control. In this work, we illustrate the workflow of our system and show accurate targeting in phantom experiments. *Ex vivo* porcine lung experiments show that our steerable needle can be tuned to achieve appreciable curvature in lung tissue. Lastly, we present targeting results with our system using two scenarios based on patient cases. In these experiments, phantoms were created from patient-specific computed tomography information and our system was used to target the locations of suspicious nodules, illustrating the ability of our system to reach sites that are traditionally inaccessible transorally.

Keywords: Surgical robotics; concentric tube robot; steerable needle; minimally-invasive lung biopsy.

JMRR

1. Introduction

More lives are lost to lung cancer in the US than any other type of cancer (≈ 160,000 in 2014) [1], and early diagnosis is critical to survival. Patients diagnosed with lung cancer in Stage I have an 88% 10-year survival rate [2], while Stage III or IV patients have only a 15% 5-year survival rate [3]. In order to obtain a definitive diagnosis, a biopsy is required for suspicious nodules identified in CT scans. Unfortunately, nodules (which may or may not be cancerous) often develop in the peripheral regions of the lung and are difficult to access for biopsy, leaving some patients with no safe option for definitive diagnosis.

The two most common biopsy procedures used to attempt to reach these suspicious nodules are a

*This material is based upon work supported by the National Institutes of Health under award R21 EB017952 and the National Science Foundation under awards IIS-1054331 and IIS-1149965 as well as two NSF Graduate Research Fellowships. Any opinions, findings, and conclusions or recommendations expressed in this material are those of the authors and do not necessarily reflect the views of the NIH or the NSF.

Received 27 October 2015; Revised 23 December 2015; Accepted 11 February 2016; Published 11 October 2016. This paper was recommended for publication in its revised form by Editor Mahdi Tavakoli.
Email Addresses: ‖*philip.j.swaney@vanderbilt.edu*, **ron@cs.unc.edu, ††*robert.webster@vanderbilt.edu*

percutaneous approach and a transoral bronchoscopic approach. Percutaneous transthoracic needle biopsy is a well-established method with high diagnostic yield for large nodules, but it requires puncturing the pleura (the membrane surrounding the lung). Thus, it carries a significant risk of pneumothorax (lung collapse), a severe and possibly deadly complication that develops in up to 25% of percutaneous biopsies [4]. Other reported complications include pulmonary hemorrhage, pleuritic chest pain, and vasovagal reaction [5]. In addition to these complications, percutaneous biopsy has a low diagnostic yield ($< 52\%$) for small nodules under 1.5 cm in diameter [6].

In contrast to percutaneous needle biopsy, bronchoscopic approaches are less invasive, carry a significantly lower risk of pneumothorax (bronchoscopes do not puncture the pleura), and may be the only biopsy option for patients with co-morbidities such as chronic obstructive pulmonary disease (COPD). Bronchoscopes are standard medical devices that are deployed transorally. They are typically made with a flexible shaft and a tendon-driven tip that bends when the tendons are actuated using levers on the handle, steering the tip of the bronchoscope [7]. The main drawback of bronchoscopic biopsy is that the bronchoscope can only move through the lung's bronchial tree, and even then, only in the larger bronchi due to the bronchoscope's diameter. This limits the number of nodules that can be biopsied to those within the larger bronchi or in close proximity to them. Furthermore, the diagnostic yield of bronchoscopy falls off significantly the further the nodule is located from the entrance to the lung (82%, 61%, and 53% for central, intermediate, and peripheral nodules, respectively), and the diagnostic yield for small nodules (< 2 cm) is only 23% [8]. Although bronchoscopic biopsy is safer and less invasive for the patient, these limitations curb the use of bronchoscopy and make it clear that a better transoral approach is needed.

Recently, groups have augmented bronchoscopes with image-guidance, attempting to improve bronchoscopic biopsy (see [9] for a review). The three main approaches are virtual bronchoscopy, eletromagnetic (EM) guidance, and endobronchial ultrasound (EBUS). Virtual bronchoscopy displays a virtual model of the airway that is segmented from preoperative CT images and registered to the live image feed of the bronchoscope, enabling navigational cues to be overlaid on the model [10]. However, even with the benefit of navigational guidance, this approach presents some of the same access limitations as traditional bronchoscopy, notably the inability to travel outside of the bronchi. In EM guidance, small magnetically-tracked instruments are deployed through the bronchoscope and travel further through the bronchial tree than standard bronchoscopes [11,12]. Nonetheless, these devices are still only intended to move through the bronchial tree and access nodules that are located within the bronchi or in close proximity to them. Furthermore, the diagnostic yield of these systems is only 63–74% for nodules averaging 2.3 cm [13–16] (it is also worth noting that these statistics do not include nodules for which no attempt is made due to difficulty of access). One group has recently used a bronchoscopically deployed needle and tunneling sheath under fluoroscopic guidance to create a path to nodules located outside of the bronchial tree [17]. However, the authors note that the device is limited to nodules that are reachable by an obstacle-free (i.e. avoiding critical blood vessels and other sensitive structures) straight-line path. Another promising emerging technology is EBUS in which ultrasound is used to either locally guide the placement of a guide sheath for biopsy [18] or provide image feedback for the deployment of a straight needle from the tip of a bronchoscope [9]. Since our system can, in principle, be used with any guidance modality that can provide the locations of both the target and needle tip, it could potentially be used in conjunction with EBUS in the future to provide steerability to EBUS-guided needles.

Our system uses concentric tube robots and bevel steered needles to increase the capabilities of standard bronchoscopes (see Fig. 1). Concentric tube robots are made from a series of precurved, superelastic tubes that translate and rotate inside one another to create curvilinear motion. Concentric tube devices were some of the first devices made from nitinol during the 1980s [19]. Originally thought of exclusively as needles, in 2006 they were proposed as needle-scale manipulators [20, 21], kicking off a period of active modeling research that resulted in the model typically used today [22, 23]. These robots have been applied in a variety of surgical contexts including endonasal surgery [24], cardiac procedures [25], prostate resection and brachytherapy [26, 27], and retinal vein cannulation [28]. In the lung, there has been work done on planning obstacle-free paths through the bronchi using only concentric tube robots [29]. It has also been shown that concentric tube robots can augment the dexterity of both rigid [26] and flexible [30] endoscopes. In our system, we use this added dexterity to orient and deploy a bevel tip steerable needle.

Bevel steered needles are made using a flexible needle shaft and an asymmetric tip that causes the needle to bend in a controllable fashion upon insertion into tissue [32]. The field of needle steering has been active for over 10 years and has seen numerous advancements including motion controllers, motion planning, and needle tip design (see [33, 34] for reviews). With our system, we use bevel tip needle steering for its simplicity and feasibility when deployed through a long, thin pathway. We also incorporate a new type of steerable needle with our system, called the flexure-tip needle [35]. This needle achieves high curvature while reducing tissue damage when compared to other high-curvature tip designs

(e.g. kinked-tip needles [35]), and can be deployed through a narrow working channel.

This paper makes a number of contributions to the state of the art. Perhaps most important is our overall system concept in which three kinds of continuum devices are unified to provide a way to access the peripheral lung transorally. This is the first system where concentric tube robots have been used to deploy bevel tip steerable needles, two devices that have previously been studied extensively individually. It is also the first system to physically deploy concentric tube robots from a bronchoscope, which is needed to enable practical application of prior simulation and planning algorithms for concentric tube robots in the lung [36, 37]. Experimental contributions include validating that the sliding mode controller of [38] works with the flexure-tip needle of [35] (the controller had previously been used only with traditional bevel tip needles), and experiments validating aspects of our system using anatomical patient data and *ex vivo* tissue. Preliminary versions of some results described in this manuscript have appeared previously in conference form [39, 40]. Here, we provide an archival unification of these results, and extend them with additional phantom targeting experiments (Sec. 5.1), a new *ex vivo* bronchial piercing experiment (Sec. 5.2), a demonstration that a flexure-tip needle can achieve appreciable curvature in *ex vivo* lung tissue (Sec. 5.3), and a new set of phantom experiments based on real patient cases (Sec. 5.4).

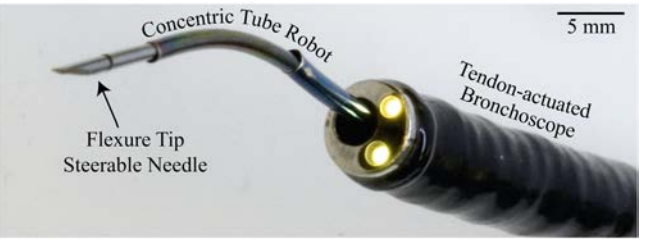

(a)

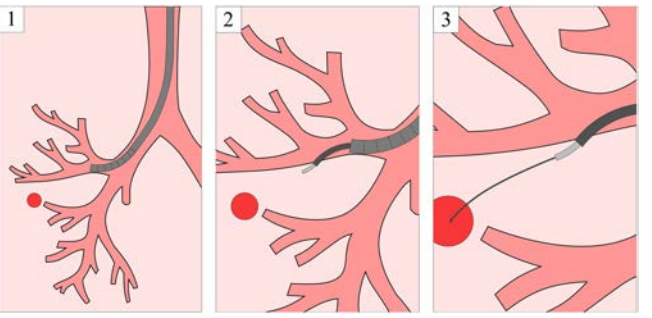

(b)

Fig. 1. (a) Our system combines a tendon-actuated bronchoscope, a concentric tube robot, and a bevel steered needle to reach locations throughout the lung transorally. (b) The deployment steps for our combined system involve (1) deploying the bronchoscope to a desired site in the bronchial tree, (2) deploying the concentric-tube robot from the bronchoscope working channel to the bronchial wall, piercing through the wall, and entering the lung parenchyma and (3) steering the flexure-tip needle to the target under closed-loop control.

2. System Overview and Workflow

Our system (Fig. 1(a)) aims to expand the capabilities of a transoral approach by adding the ability to reach nodules located far from the bronchi through the integration of a concentric tube robot and a bevel tip steerable needle with a standard tendon-actuated bronchoscope. In our system, the physician first inserts a tendon-actuated bronchoscope to an accessible location en route to the nodule. A concentric tube robot then deploys through the bronchoscope and passes through the bronchial wall, providing access to nodules located in the lung parenchyma (the tissue surrounding the bronchi). Lastly, a steerable needle deploys through the concentric tube robot and drives through the lung tissue to the nodule. This approach will enable access to nodules located in the parenchyma of the lung with less risk of pneumothorax, since the pleura surrounding the lung is never damaged. A prototype of our system is shown in Fig. 2 and the deployment of the three stages of the device is illustrated in Fig. 3. The intended insertion workflow is detailed below:

(1) The surgeon deploys the bronchoscope transorally using standard practices. An Olympus BF 1T30 (Olympus, USA) bronchoscope was used for this work.
(2) The concentric tube robot extends from the tip of the bronchoscope and moves toward the bronchial wall.
(3) A sharp nitinol wire, which we will henceforth refer to as the "piercing needle," deploys through the concentric tube robot and creates an opening in the bronchial wall using a spring-loaded piercing mechanism. The concentric tube robot is advanced over the piercing needle and through the bronchial wall, and the piercing needle is then removed.
(4) The concentric tube robot aims its tip approximately toward the target nodule.
(5) The steerable needle deploys through the concentric tube robot and is guided under closed-loop control to the desired target.
(6) The surgeon advances a coaxial access sheath through the bronchoscope and over the concentric tube robot and steerable needle, creating an access channel to the target through which a biopsy can be collected or a therapeutic agent can be injected.

We foresee this surgical workflow being performed with the help of image-guidance in a future clinical version of

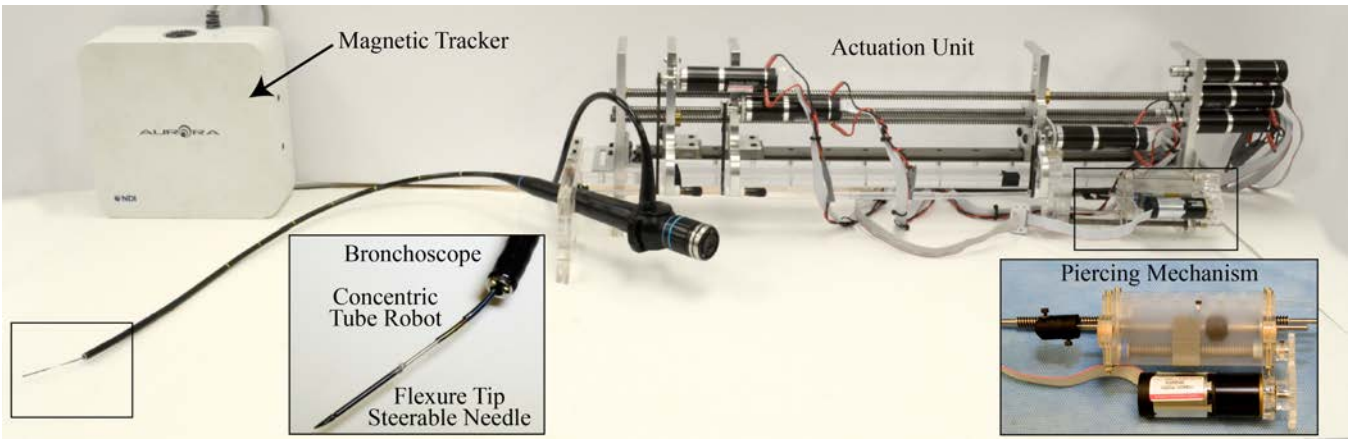

Fig. 2. The components of the three-stage steering system developed in this work are shown. The system combines a tendon-actuated flexible bronchoscope with a concentric tube robot and a flexure-tip steerable needle to provide transoral access to the peripheral lung. The actuation unit controls the concentric tube robot and steerable needle (see [31] for details on a similar actuation unit), and the piercing mechanism provides access to the lung parenchyma from the bronchial tree. Closed-loop feedback is provided by a magnetic tracking system.

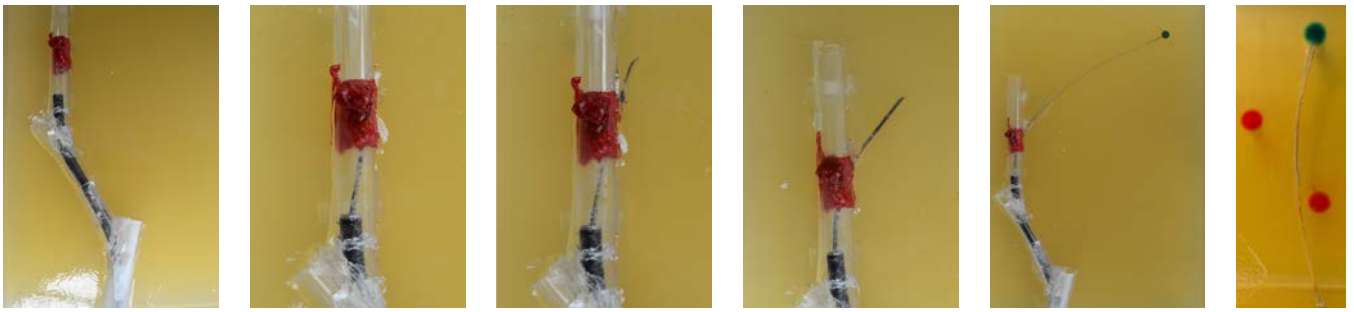

(a) (b) (c) (d) (f) (g)

Fig. 3. Pictures of the deployment steps for our lung system are shown. (a) The bronchoscope is deployed transorally into the bronchial tree. (b) Second, the concentric tube robot extends from the tip of the bronchoscope to the desired location for the opening in the bronchial wall. (c) The piercing needle then deploys through the concentric tube robot and creates the opening in the bronchial wall. (d) The concentric tube robot advances over the piercing needle and through the bronchial wall and aims in the direction of the target. (e) Next, the piercing needle is removed and the steerable needle is deployed from the concentric tube robot to the target. (f) Lastly, an access sheath is passed over the concentric tube robot and steerable needle to the target, allowing for biopsy through the sheath (see Sec. 6 for more details on the access sheath).

the system described in this paper. There are two potential imaging approaches that could be used. The first involves taking a preoperative scan of the lung that will be used to identify the target nodule and plan the location of the opening in the bronchial wall and the desired needle path. This preoperative information would then be coupled with intraoperative magnetic tracking feedback for closed-loop control. This approach will require registration between the preoperative and intraoperative data, which is already done in current image-guided lung systems [11, 12]. The other potential approach is to perform the whole deployment with intraoperative imaging such as real-time CT (CT Fluoroscopy) or MRI. In addition to visualizing the system and target during the procedure, this approach would also allow us to see obstacles and critical structures along the deployment path in real time. We believe that our system could be used with either of these imaging approaches. We will now discuss in more detail the devices that are deployed from the bronchoscope and enable our system to reach nodules located in the parenchyma without puncturing the pleura.

3. Concentric Tube Robot Subsystem

After the bronchoscope is guided by the physician to the desired site in the bronchial tree (step 1 in Sec. 2), the concentric tube robot is deployed out from the bronchoscope tool port. We utilize the concentric tube robot for three important purposes in our system. First, the concentric tube robot enables our system to approach

Table 1. Concentric tube robot parameters.

	Outer Tube	Inner Tube
Outside diameter (mm)	1.38	1.14
Inside diameter (mm)	1.29	0.97
Radius of curvature (mm)	25.4	17.8
Curved length (mm)	55	27
Straight length (mm)	735	833

the bronchial wall in a direction as close to perpendicular as possible, aiding with piercing the bronchial wall (step 2 in Sec. 2). Second, the concentric tube robot is used to deliver a piercing needle to the bronchial wall (step 3 in Sec. 2), creating an access port in the wall for our system to travel through. Lastly, the concentric tube robot is used to align the steerable needle such that the target nodule lies within the reachable workspace of the needle (step 4 in Sec. 2). The position of the concentric tube robot can be tracked using the same magnetic tracking coil in the steerable needle since the needle is inside the concentric tubes. The geometric parameters of the concentric tube robot used in this work can be found in Table 1. Each tube is comprised of a straight section followed by a precurved section at the distal end of the tube. For each tube, the length of each section and the radius of curvature of the precurved section is provided in Table 1.

3.1. *Deploying from the bronchoscope to the bronchial wall*

The added dexterity of the concentric tube robot coupled with the tendon-actuated bronchoscope helps in bringing the piercing needle from the bronchoscope tip to the bronchial wall (step 2 in Sec. 2). In order to assist with creating the opening in the bronchial wall using the piercing needle, it is useful to approach the wall in as nearly a perpendicular direction as possible. We use the concentric tube robot to accomplish this (see Fig. 4 for an example). The kinematics used to guide the concentric tube robot are given in [22, 23]. Depending on the desired location of the bronchial wall opening and desired orientation, the physician may choose to deploy one or both concentric tubes from the bronchoscope to the bronchial wall.

3.2. *Piercing the bronchial wall*

After reaching the desired site in the bronchial wall with the concentric tube robot, the piercing needle (a 0.78-mm diameter nitinol wire with a sharp conical tip) is deployed through the concentric tube robot (step 3 in Sec. 2). Due to the muscular tissue and cartilage rings that make up the bronchi, an impulse is needed to pierce

Fig. 4. The concentric tube robot coupled with the tendon-actuated bronchoscope provide flexibility in selecting the position and orientation of the bronchial wall opening. This added dexterity also assists with orienting the initial pose of the steerable needle. Here, the bronchoscope and concentric tube robot are deployed in a clear PVC tube to a desired bronchial target on the wall of the tube.

the wall. In order to deliver this impulse to the piercing needle, a spring-loaded piercing mechanism was designed and is shown in Fig. 5. It should be noted that creating a hole in the bronchial wall for parenchyma access and nodule targeting has been shown to be safe in initial human trials [17], and that the piercing depth of our mechanism can be set according to the physician's depth specifications to prevent piercing too deep. Upon piercing the bronchial wall, the concentric tube robot is advanced over the piercing needle and through the opening in the bronchial wall. The piercing needle is then removed, and the concentric tube robot can now deploy the steerable needle to the target.

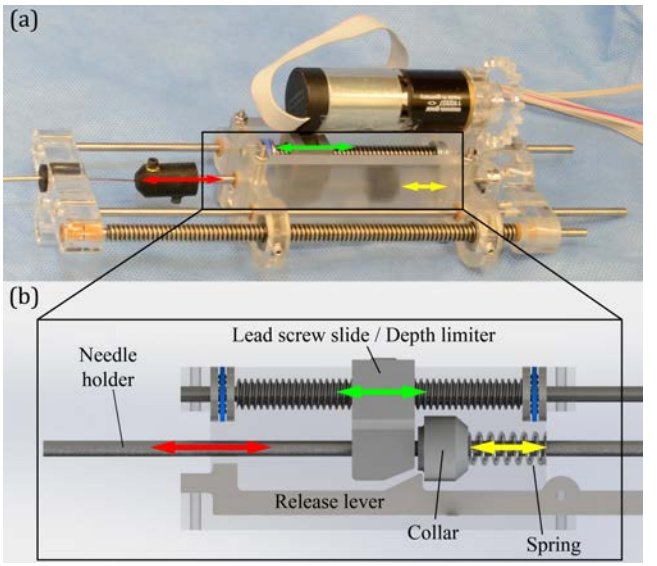

Fig. 5. (a) View of the piercing mechanism used to impart a rapid motion to the piercing needle that creates a needle-sized port in the bronchial wall. (b) In the piercing mechanism, the lead screw slide compresses a spring until the collar is secured by the release lever. Upon triggering the release lever, the needle holder is propelled forward until it contacts the lead screw slide, controlling the depth of the piercing needle.

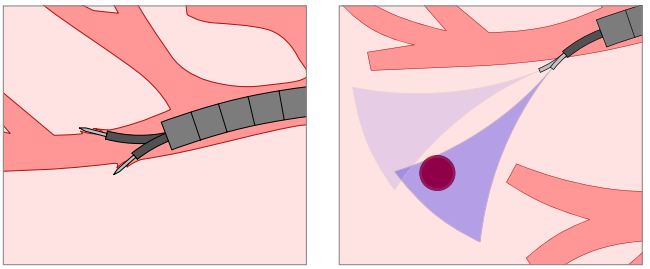

(a) (b)

Fig. 6. (a) The flexibility provided by the concentric tube robot and tendon-actuated bronchoscope when selecting the position and orientation of the bronchial wall opening and initial pose of the steerable needle is illustrated. (b) The concentric tube robot is useful for directing the steerable needle so that the target nodule is within the needle's reachable workspace. An example of adjusting the inner-most concentric tube to redirect the initial alignment of the needle in order to reach the target is illustrated.

3.3. *Aiming the steerable needle*

The concentric tube robot (and potentially the tendon-actuated bronchoscope, if additional dexterity is needed) now orient the initial pose of the steerable needle that passes through the inner concentric tube toward the target (step 4 in Sec. 2). The ideal alignment of the steerable needle is pointing directly toward the nodule, as this provides both the minimum length to the target and the maximum steerability to correct for disturbances and avoid obstacles along the path. If obstacles prevent this ideal path, the concentric tube robot can position and orient the initial alignment of the steerable needle such that the target still lies within the "trumpet shaped" workspace of the steerable needle. The needle can then drive to the target while steering to avoid obstacles along the way. An illustration of aligning a bevel steered needle with a concentric tube robot can be seen in Fig. 6. Now that the steerable needle is aligned toward the target, our system delivers the steerable needle to the target using the methods described in the following section.

4. Steerable Needle Subsystem

The steerable needle used in our system is a flexure-tip needle that consists of a beveled needle tip, a flexible needle shaft, and a flexure joint (see Fig. 1(b) and [35] for further information on this tip design). All three components are made from nitinol. When inserted into tissue, the asymmetric bevel tip creates a force that bends the flexure and causes the needle to travel in a curved trajectory through the tissue. When no load is applied to the tip, the flexure joint straightens and the needle can easily pass through the concentric tube robot. The flexure joint also straightens when axially rotated while in tissue, minimizing tissue damage when a straight trajectory is implemented via continuous axial rotation during insertion.

The flexure-tip needle we used in our system and for the phantom and anatomical validation experiments in Secs. 5.1 and 5.4 has a needle shaft with an outside diameter (OD) of 0.8 mm and an inside diameter (ID) of 0.6 mm. The bevel tip has an OD of 1.16 mm in order to house a six degree-of-freedom magnetic tracking sensor (NDI Aurora, Canada). The bevel tip itself has a length of 4 mm and a bevel angle of 15°. The flexure joint is comprised of three 0.125 mm diameter nitinol wires positioned side by side within the needle shaft (see [35] for additional illustrations of the flexure joint), and the maximum angle the flexure tip can bend is 20°. The length of the entire needle is 1.21 m.

In order to accurately deliver the steerable needle through the parenchyma to the target, we use the sliding mode controller developed by Rucker *et al.* [38]. Magnetic tracking sensors provide closed-loop feedback of the needle tip pose to the controller. In [38], the controller was validated in the context of reaching target points, trajectory following, and targeting objects that are moving or deforming within the tissue, perhaps due to respiration. In [38] the controller was tested with a traditional bevel tip needle, so a novel contribution of the experiments in this paper is verifying that the controller also works for the high curvature and tissue sparing flexure-tip needle design.

5. Experiments

The first set of experiments we performed tested the ability of our system to maneuver in a bronchial tree and deploy the concentric tube robot from the bronchoscope. We then validated the use of the sliding mode controller with the flexure-tip steerable needle and tested the accuracy of our system at delivering the steerable needle to a selected target in a phantom model. After testing the basic deployment concept and targeting accuracy of our system, we experimented with our system in biological and anatomical models to verify use of the system when interacting with realistic tissue and anatomy.

5.1. *System feasibility & accuracy experiments*

In order to test the ability of our system to maneuver in the bronchi and deploy the concentric tube robot, we constructed a phantom bronchial tree model using PVC plastic tubes. Each successive bronchial tube is smaller than the one it extends from, mimicking the structure of the human bronchi. An access hole was cut into the side of the PVC in the third bronchial tube to allow the concentric tubes and steerable needle to exit the phantom.

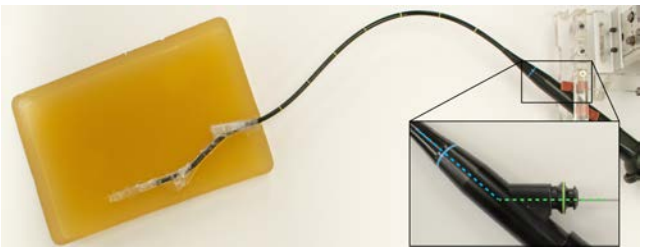

Fig. 7. The experimental setup used for the system feasibility and accuracy experiments as described in Sec. 5.1 consisted of a phantom bronchial tree (made from plastic tubes) that was embedded in phantom parenchyma (gelatin). The inset shows the bronchoscope handle and the sharp bend in the working channel, which is discussed further in Sec. 6.

The bronchial tree model was then embedded in gelatin to simulate the support structure of the lung, including the parenchyma (see Fig. 7 for experimental setup). The gelatin was made from 10% by weight Knox gelatin (Kraft Foods Global, Inc., USA). The bronchoscope, with the concentric tube robot passing through the working channel, was then deployed through the phantom bronchial tree to a site roughly 1 cm from the access hole. The concentic tube robot was then extended from the bronchoscope up to the gelatin, confirming the system's ability to deploy a concentric tube robot through the flexible bronchoscope as described in Sec. 2.

After deploying the bronchoscope and concentric tube robot through the phantom bronchial tree, we validated the use of the sliding mode controller with the flexure-tip steerable needle described in Sec. 4, testing the accuracy of our system at delivering the steerable needle to a selected target. The flexure-tip needle with the six-degree-of-freedom tracking coil embedded in its tip was loaded into the system, passing through the concentric tube robot and bronchoscope. The concentric tube robot was positioned in the gelatin such that the steerable needle was aiming in the general direction of the target. The flexure-tip steerable needle was then controlled through the gelatin to the target using the sliding mode controller with magnetic tracker feedback. A total of 21 targeting experiments were performed. The targeting results can be seen in Fig. 8.

5.2. *Bronchial wall piercing of ex vivo porcine tissue*

In order to verify the ability of our piercing mechanism to perform its intended task, we excised a section of bronchial tube from a porcine lung (≈ 1.50 mm wall thickness) and affixed the tissue sample over the access hole in the plastic phantom bronchial tree using cyanoacrylate glue. The bronchoscope and concentric tube robot were deployed to the bronchial wall as described in Sec. 2, and the piercing mechanism then fired the piercing needle to create an access hole in the bronchial tissue. The result of this experiment can be seen in Fig. 9(a). Various thicknesses (between 1.15–2.5 mm wall thickness) of *in situ* porcine lung bronchi were successfully pierced (see Fig. 9(b) for an example).

5.3. *Needle deflection in ex vivo porcine tissue*

Another important feature of our system is the ability to steer the flexure-tip needle through the parenchyma. It is commonly assumed in the bevel tip needle steering literature that one can match needle properties (bevel angle, shaft stiffness, etc.) to any biological tissue of interest in order to achieve appreciable curvature. While examples do exist of needles that have achieved appreciable curvature in brain [41], liver [42], kidney [42], and muscle [32], designing a needle for a new tissue type is not trivial. It requires substantial iterative experimentation, since curvature is sensitive to a variety of needle design parameters. Thus, rather than leave to future work verification that a needle design exists that can achieve appreciable curvature in lung, we set out to find a needle design that could achieve curvatures that provide a reasonable needle workspace (see Fig. 6(b)).

To confirm that we can design such a flexure-tip needle, we performed a series of open-loop *ex vivo* experiments. In the first set of experiments, we con-

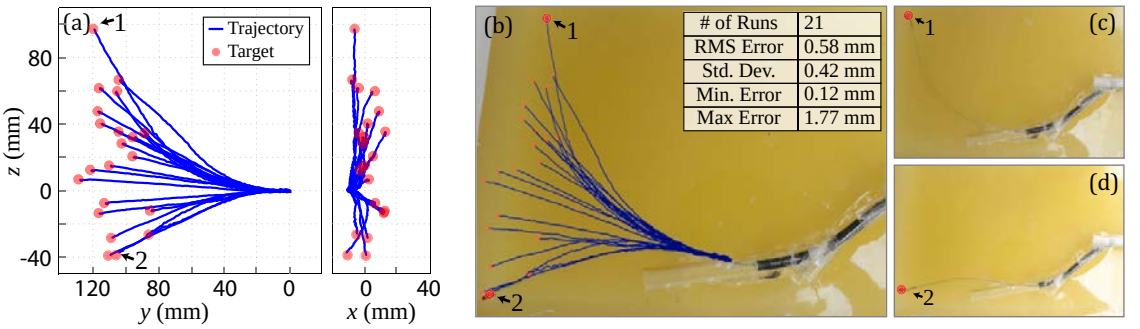

Fig. 8. (a) Phantom targeting experimental results of 21 insertions as described in Sec. 5.1. (b) The 21 targeting trials are overlaid on the experimental setup. Trials 1 and 2 are explicitly shown in (c) and (d).

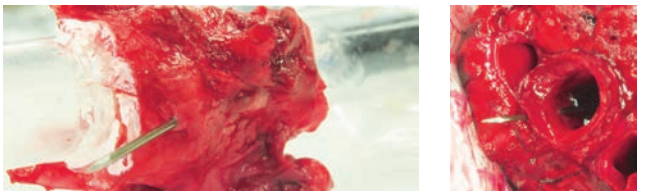

(a) (b)

Fig. 9. (a) *Ex vivo* porcine bronchial tissue was wrapped around a PVC tube representing a bronchial tube. The piercing mechanism was used to fire the piercing needle through the tissue, as shown here. This creates a port in the bronchial wall for the concentric tube robot and steerable needle to deploy through. (b) The piercing mechanism was also tested in whole samples of porcine lung, shown here.

structed two pre-bent nitinol needles (i.e. needles where the flexure hinge has been replaced by a permanent bend [42]) with fixed tip angles of 25° and 45° (the 45° needle is shown in Fig. 10(a)). Each needle was inserted into the porcine lung sample five times. The measured radius of curvature (RC) and standard deviation (SD) are reported in Table 2(a). The results indicate that a tip angle of 45° produces a smaller radius of curvature than the same needle with 25°.

(a) (b) (c)

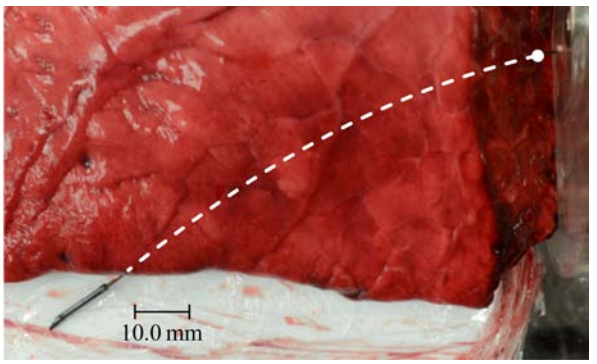

(d)

Fig. 10. The three needles used for the *ex vivo* porcine lung insertion experiments with results presented in Table 2. (a) The 45° pre-bent needle. (b) and (c) The two flexure-tip needles. The flexure-tip needle shown in (c) produced paths with the smallest radius of curvature, and a representative path generated by the same needle is shown in (d).

Table 2. *Ex vivo* flexure-tip needle testing results.

(a) Pre-bent Needle (Fig. 10(a))

Wire Dia.	Tip Angle	Tip Len.	RC	SD
0.558 mm	25°	2.9 mm	733.4 mm	109.2 mm
0.558 mm	45°	2.9 mm	268.1 mm	164.6 mm

(b) Flexure-tip tube needle 1 (Fig. 10(b))

Tube O.D.	Tube I.D.	Tip Len.	RC	SD
0.8 mm	0.6 mm	4.2 mm	717.5 mm	243.2 mm
Bev. Angle	Max Angle	Flex. Wires		
10°	45°	3		

(c) Flexure-tip wire needle 1 (Fig. 10(c))

Wire Dia.	Tip Dia.	Tip Len.	RC	SD
0.51 mm	1.16 mm	3.0 mm	255.0 mm	66.2 mm
Bev. Angle	Max Angle	Flex. Wires		
30°	45°	2		

Measured RC in porcine parenchyma. The average RC and SD of $n = 5$ open-loop needle insertion trials into *ex vivo* porcine lung for (a) two pre-bent needles, and (b), (c) two flexure-tip needles (shown in Fig. 10). The wire diameter (Wire Dia.) measures the external diameter of the shaft wire, the bevel angle (Bev. Angle) measures the angle of the bevel tip relative to the longitudinal axis of the shaft, the tip length (Tip Len.) measures the length of the needle tip after the pre-bend in the shaft or the length of the flexure-tip after the flexure, the tip diameter measures the external diameter of the tip flexure joint assembly, the maximum angle (Max Angle) measures the maximum angle the flexure tip can deflect, and the number of flexure joint wires (Flex. Wires) describe the number of 0.125 mm diameter nitinol wires used to create the flexure joint.

Using the results of the pre-bent needles as a coarse guide, we constructed two new flexure-tip needles with varying geometry (see Figs. 10(b) and 10(c)) that each had a maximum flexure angle of 45°. These new needles employed the same basic flexure design as the needle used in Secs. 5.1 and 5.4, but with different needle parameters (e.g. number of flexure wires and tip diameter) selected for lung tissue, in contrast to the gelatin used prior. The results of five open-loop insertion trials are presented in Tables 2(b) and 2(c) for these flexure-tip needles. The smallest radius of curvature achieved in the porcine lung sample was 255.0 mm, which was

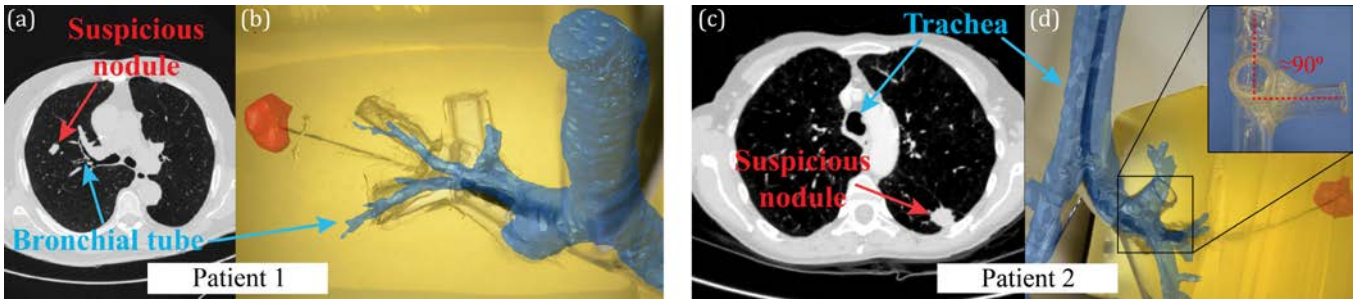

Fig. 11. Patient case studies in which our proposed system would be particularly valuable. Patient 1 (a) A suspicious nodule was located centrally in the lung, away from both the bronchial tree and the lung surface. We segmented the bronchial tree and the nodule, and built a phantom to model the anatomy. (b) The segmented anatomy is overlaid on the phantom model. In three trials, the nodule was targeted with an average of 1.33 mm tip error. Patient 2 (c) A suspicious nodule was located in the periphery of the lung, far from the bronchial tree. The bronchial anatomy was segmented, and a phantom model built based on the anatomy. (d) The segmented model is overlaid on the phantom model, and in three trials the nodule was targeted with an average of 2.02 mm tip error. The inset shows the 90° bend in the bronchus that our system traversed.

obtained by the needle whose results are presented in Table 2(c) and shown in Fig. 10(c). A representative path produced by this needle is shown in Fig. 10(d).

5.4. *Anatomical case studies*

Lastly, to illustrate the benefits of our system at reaching targets that are difficult or impossible to reach transorally, we present two scenarios based on actual clinical cases of patients with suspicious lung nodules treated at Vanderbilt University Medical Center. Based on their experience, the clinicians in both cases determined that the nodules could not be safely reached via a transoral bronchoscopic approach. The decisions were made based on the location of the nodule, the condition of the patient, and other factors. De-identified CT scans of the patients were used to create the anatomical models. We segmented the bronchial tree and nodule for each patient, and plastic PVC phantom bronchial trees were created (in the same manner as Sec. 5.1) to approximately (as near as could be judged by eye, when hand-gluing tube sections together) replicate the geometry of the segmented bronchial structure. The bronchial phantoms were set in gelatin and three locations within each nodule were targeted. The target locations in the gelatin phantom were approximated using the relative location of the nodule centroid with respect to the bronchial tree in the CT scans. The two clinical scenarios are as follows.

5.4.1. *Patient 1 — Centrally-located nodule*

Patient 1 is a 72 year old former smoker with a right upper lobe nodule that was suspected of being malignant (see Fig. 11(a)). This patient underwent traditional bronchoscopy as well as a percutaneous CT-guided biopsy. Both attempts were unsuccessful at accurately reaching the nodule, since the nodule was located too far away from an access bronchial tube for bronchoscopy and was too deep for accurate localization using a percutaneous approach. This scenario motivates our system, since it can target nodules that are not immediately adjacent to an access bronchi without puncturing the pleura and the associated risk of pneumothorax. In our anatomical model, we targeted the nodule three times with an average tip error of 1.33 mm (see Fig. 11(b) for an experimental run).

5.4.2. *Patient 2 — Peripherally located nodule*

Patient 2 is a 68 year old current smoker with COPD and a suspicious pleural-based pulmonary nodule located in the periphery of the left lower lobe (see Fig. 11(c)). This nodule was not able to be accessed with a traditional bronchoscope because of its peripheral location in the lung. While this nodule was relatively easy to access using a percutaneous approach, the patient's COPD increases the risk of a biopsy-induced pneumothorax. In this scenario, it would be safer if the biopsy were performed with the bronchoscopic approach we propose, eliminating the need for a pleural puncture. Note that we selected this case as an example of one that would be challenging for our system, due to the 90° bend the bronchoscope was required to navigate (see Fig. 11(d)). Yet even in this challenging case, our system was able to target the phantom nodule three times with an average tip error of 2.02 mm.

6. Discussion

The robotic system and workflow presented in this paper for targeting suspicious lung nodules has the potential to save lives by enabling earlier stage diagnosis via accurate

targeting and minimizing the risk of pneumothorax (lung collapse). While healthy patients usually recover from pneumothorax, it is a serious complication for all patients, and is potentially life threatening for patients with comorbidities or reduced lung function. We anticipate that our system will have a higher yield rate than existing percutaneous and transoral approaches because our biopsy needle is both steerable and controllable in a closed-loop manner, which we expect will result in more accurate targeting (which is particularly important for small nodules). Our approach also has an added benefit over current augmented bronchoscopic approaches in that we anticipate it will enable nodules that are in the periphery of the lung to be targeted transorally, thus broadening the reach of bronchoscopic methods. In this paper, we have demonstrated accurate targeting in gelatin phantoms, as well as successful piercing of porcine bronchial wall and needle deflection in porcine lung tissue. While this work aims to show the feasibility of our combined system and approach, there are also a number of challenges to overcome and opportunities for future research.

One challenge we encountered related to the process of inserting the concentric tube robot and steerable needle through the bronchoscope. The bronchoscope's working channel had a sharp bend in the handle, which makes it challenging to guide tubes through it (see inset in Fig. 7). To overcome this, we inserted a thin-walled polytetrafluoroethylene (PTFE) sheath through the working channel, and then inserted our concentric tube robot and steerable needle through this. Even with this sheath, the bend in the handle was sufficiently sharp that caused mild plastic deformation of the tubes. Since this is only problematic if the deformation occurs at the tip of the tubes, we loaded the concentric tube robot and steerable needle from the tip of the bronchoscope before inserting it into the bronchial tree. In future work, it may be useful to partner with a bronchoscope manufacturer to create a bronchoscope with a straighter working channel to alleviate this challenge.

Since we ultimately intend to use a guide sheath passed over the concentric tube robot and steerable needle to perform a biopsy and/or deliver therapy, we can use the same PTFE guide sheath we passed through the bronchoscope for this purpose. Toward this end, we performed a simple validation experiment in which we passed a PTFE sheath over the flexure-tip steerable needle once it had reached the desired target site. We then removed the steerable needle, leaving the guide sheath in place, and inserted a flexible biopsy tool through the sheath to obtain core samples of the gelatin target. The result of this preliminary study can be seen in Fig. 12.

Another more minor challenge we overcame in this research is that the concentric tube robot and steerable needle can stiffen the tip of the bronchoscope. Even

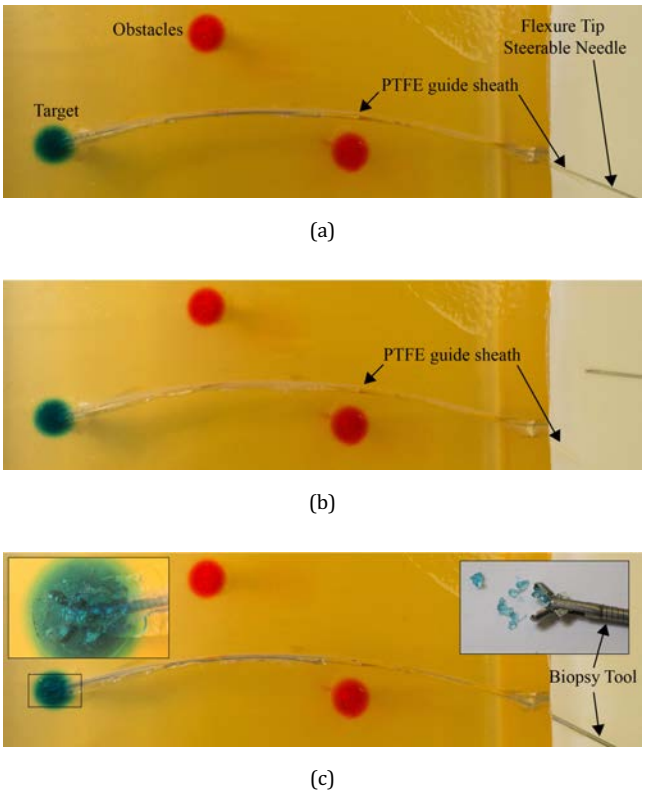

Fig. 12. A preliminary investigation into the use of a guide sheath for biopsy is shown. (a) First, a PTFE guide sheath was passed over a flexure-tip steerable needle that had reached the target, (b) the needle was removed through the sheath, creating a path to the target, (c) then a flexible biopsy tool was inserted through the guide sheath and used to obtain core samples of the gelatin target.

though the tendons can overcome this and still deflect the tip, doing so will require more force on the bronchoscope control levers. Thus, so that the bronchoscope feels to the operator like it does in current clinical practice, we retracted the tubes and needle past the bending tip of the bronchoscope before deploying it through the bronchi. Also, due to the long length of the bronchoscope, our steerable needle shaft must be quite long (121 cm), and torsional windup due to friction between the tubes can become a problem. In order to alleviate this, we used a 6 degree-of-freedom magnetic tracking sensor, providing the full needle-tip pose to the sliding mode controller. This allows us to ignore the torsional windup of the needle shaft and gives us accurate steering results.

Although we envision the physician deploying the bronchoscope manually in our system, it may be useful to investigate roboticizing bronchoscope deployment in the future (see e.g. [43]), particularly if a robotic system can maneuver the scope more accurately and reliably than a human. However, it is desirable from a clinical adoption and cost standpoint to rely on manual deployment, and

thereby minimally impact the established workflow of bronchoscopy. It is also worth noting that our system could be used in conjunction with virtual bronchoscopy [10] to assist the physician with manually navigating the bronchial tree. We also intend to reduce the size of our actuation unit in the future, as the specific prototype shown in Fig. 2 was built as a bench-top system for the initial validation of our approach presented here. In the next prototype, we intend to miniaturize the actuation mechanism and simplify the electronics, similar to the design presented in [44]. Even if weight cannot be minimized sufficiently for a long procedure, we note that it is possible to use a passive support arm to relieve the physician of the device's weight, in a manner similar to the system described in [44].

The system we present in this work utilizes the bronchoscope, concentric tube robot, and steerable needle to achieve accurate targeting. We note that in some instances under ideal conditions, it may be possible for the bronchoscope and steerable needle alone to accomplish the procedure. In anatomically favorable cases, one or both concentric tubes could potentially be removed, simplifying the system. Additionally, under ideal conditions, it may be possible to use the bronchoscope and the concentric tube robot to reach the target. While concentric tube robots have been shown to "follow-the-leader" with appropriately selected tube precurvatures and deployment sequences [45], the long transmission lengths required to pass the concentric tube robot through the bronchoscope will make it difficult to keep the concentric tubes stable. Nonannular concentric tubes can help overcome this instability [46], but concentric tube robots deployed in a "follow-the-leader" manner may have trouble correcting for misalignment or unmodeled deflection of the tubes. Ultimately, the use of the bronchoscope, concentric tube robot, and steerable needle together provide redundancy that is useful for targeting nodules throughout the lung, especially in the presence of modeling uncertainty, tissue deformation, and breathing.

In the future, additional experiments will be carried out on perfused, inflated porcine lungs to validate the steerable needle, controller, and system as a whole, when targeting nodules in biological tissue. This will allow us to test our system with respiratory motion, cardiac motion, and tissue inhomogeneity. These tests will also be performed with guidance from CT images. Testing with inhomogeneous biological tissue will also show the effect that tissue forces have on our overall system accuracy, although the sliding mode controller has been shown to be robust to unmodeled deflection [38]. It may also be possible to pierce the bronchial wall with the beveled flexure-tip needle, simplifying the system and removing the need for the conical tip piercing needle. Another open area of research for our system involves optimizing the design of concentric tube robots based on anatomical constraints. There is a large design space available to concentric tube robots, and work is being done to answer the challenging question of optimal tube design [37,47–49]. While these tasks are left for future work, we are optimistic that our system will perform well due to previously published results, such as needle steering in biological tissue using the same sliding mode controller we used in this work [38] and existing bronchoscopic systems employing guide sheaths to provide access to suspicious nodules [9].

7. Conclusion

In this paper, we have described a robotic system designed to accurately target suspicious nodules located in the lung. This design utilizes three separate types of continuum mechanisms and is the first system that combines a tendon-actuated device, a concentric tube robot, and a steerable needle into one system. The experiments illustrate how such a system could be beneficial for biopsy of suspicious nodules in the lung without puncturing the pleura, especially when the nodules are located far from the bronchial tree. The ability to definitively biopsy these nodules is an important healthcare challenge that will rapidly grow in importance in the next few years, based on the U.S. Preventative Services Task Force's new recommendation of yearly low-dose CT screening in high risk individuals [50]. This recommendation means that millions more suspicious nodules will be identified each year that will require biopsies for definitive diagnosis. Thus, a robotic system that can accurately target any location within the lung is urgently needed, and the system described in this paper may one day provide physicians with just such a tool.

References

1. American Cancer Society, Cancer facts & figures 2014, tech. rep., American Cancer Society (2014).
2. The International Early Lung Cancer Action Program Investigators, Survival of patients with stage I lung cancer detected on CT screening, *The New England J. Med.* **355**(17) (2006) 1763–1771.
3. M. J. Horner, L. A. G. Ries, M. Krapcho, N. Neyman, R. Aminou, N. Howlader, S. F. Altekruse, E. J. Feuer, L. Huang, A. Mariotto, B. A. Miller, D. R. Lewis, M. P. Eisner, D. G. Stinchcomb and B. K. Edwards, SEER cancer statistics review, 1975–2006, National Cancer Institute. Bethesda, MD Available: http://seer.cancer.gov/csr/ (2009).
4. J. S. Wang Memoli, P. J. Nietert and G. A. Silvestri, Meta-analysis of guided bronchoscopy for the evaluation of the pulmonary nodule, *Chest* **142**(2) (2012) 385–393.
5. G. Krishna and M. K. Gould, Minimally invasive techniques for the diagnosis of peripheral pulmonary nodules, *Curr. Opin. Pulm. Med.* **14** (2008) 282–286.
6. N. Kothary, L. Lock, D. Y. Sze and L. V. Hofmann, Computed tomography–guided percutaneous needle biopsy of pulmonary nodules: impact of nodule size on diagnostic accuracy, *Clin. Lung Cancer* **10**(5) (2009) 360–363.

7. T. Miyazawa, History of the flexible bronchoscope, in *Progress in Respiratory Research: Interventional Bronchoscopy*. Basel: Krager (2000), pp. 16–21.
8. W. A. Baaklini, M. A. Reinoso, A. B. Gorin, A. Sharafkaneh and P. Manian, Diagnostic yield of fiberoptic bronchoscopy in evaluating solitary pulmonary nodules, *CHEST J.* **117**(4) (2000) 1049–1054.
9. C. Gilbert, J. Akulian, R. Ortiz, H. Lee and L. Yarmus, Novel bronchoscopic strategies for the diagnosis of peripheral lung lesions: Present techniques and future directions, *Respirology* **19**(5) (2014) 636–644.
10. S. A. Merritt, J. D. Gibbs, K.-C. Yu, V. Patel, L. Rai, D. C. Cornish, R. Bascom and W. E. Higgins, Image-guided bronchoscopy for peripheral lung lesions: A phantom study, *CHEST* **134**(5) (2008) 1017–1026.
11. SuperDimension, SuperDimension i-Logic System Available: http://www.superdimension.com (2010).
12. Veran Medical Technologies, SPiNView Available: http://www.veranmedical.com/spinview.html (2012).
13. T. R. Gildea, P. J. Mazzone, D. Karnak, M. Meziane and A. C. Mehta, Electromagnetic navigation diagnostic bronchoscopy: A prospective study, *Am. J. Resp. Crit. Care Med.* **174**(9) (2006) 982–989.
14. D. Makris, A. Scherpereel, S. Leroy, B. Bouchindhomme, J.-B. Faivre, J. Remy, P. Ramon and C.-H. Marquette, Electromagnetic navigation diagnostic bronchoscopy for small peripheral lung lesions, *The Eur. Resp. J.* **29**(6) (2007) 1187–1192.
15. R. Eberhardt, D. Anantham, F. Herth, D. Feller-Kopman and A. Ernst, Electromagnetic navigation diagnostic bronchoscopy in peripheral lung lesions, *Chest* **131**(6) (2007) 1800–1805.
16. W. Krimsky and L. M. Seijo, Bronchoscopy and the peripheral nodule in the age of lung cancer screening and targeted therapies, *Curr. Resp. Care Reports* **1**(1) (2012) 67–71.
17. F. J. Herth, R. Eberhardt, D. Sterman, G. A. Silvestri, H. Hoffmann and P. L. Shah, Bronchoscopic transparenchymal nodule access (BTPNA): First in human trial of a novel procedure for sampling solitary pulmonary nodules, *Thorax* **70**(4) (2015) 326–332.
18. M. Takai, T. Izumo, C. Chavez, T. Tsuchida and S. Sasada, Transbronchial needle aspiration through a guide sheath with endobronchial ultrasonography (GS-TBNA) for peripheral pulmonary lesions, *Ann. Thoracic Cardiovas. Surg.* **20**(1) (2014) 19–25.
19. H. B. Gilbert, D. C. Rucker and R. J. Webster III, Concentric tube robots: State of the art and future directions, in *16th Int. Symp. Robotics Research (2013). Springer Tracts in Advanced Robotics* (in press).
20. R. J. Webster III, A. M. Okamura and N. J. Cowan, Toward active cannulas: Miniature snake-like surgical robots, in *IEEE/RSJ Int. Conf. Intelligent Robots and Systems (IROS)*, Beijing, China, October 9–15 2006, pp. 2857–2863.
21. P. Sears and P. Dupont, A steerable needle technology using curved concentric tubes, in *IEEE/RSJ Int. Conf. Intelligent Robots and Systems*, IEEE (2006), pp. 2850–2856.
22. D. C. Rucker, B. A. Jones and R. J. Webster III, A geometrically exact model for externally loaded concentric tube continuum robots, *IEEE Trans. Robot.* **26**(5) (2010) 769–780.
23. P. E. Dupont, J. Lock, B. Itkowitz and E. Butler, Design and control of concentric-tube robots, *IEEE Trans. Robot.* **26**(2) (2010) 209–225.
24. J. Burgner, D. C. Rucker, H. B. Gilbert, P. J. Swaney, P. T. Russell, K. D. Weaver and R. J. Webster III, A telerobotic systit for transnasal surgery, *IEEE Trans. Mechatron.* **19**(3) (2014) 996–1006.
25. A. H. Gosline, N. V. Vasilyev, E. J. Butler, C. Folk, A. Cohen, R. Chen, N. Lang, P. J. Del Nido and P. E. Dupont, Percutaneous intracardiac beating-heart surgery using metal mems tissue approximation tools, *Int. J. Robot. Res.* **31**(9) (2012) 1081–1093.
26. R. J. Hendrick, S. D. Herrell and R. J. Webster III, A multi-arm handheld robotic systit for transurethral laser prostate surgery, in *IEEE Int. Conf. Robot. Autom.* (2014), pp. 2850–2855.
27. M. Torabi, R. Gupta and C. Walsh, Compact robotically steerable image-guided instrument for multi-adjacent-point (map) targeting, *IEEE Trans. Robot.* **30**(4) (2014) 802–815.
28. H. Yu, J.-H. Shen, K. Joos and N. Simaan, Design, calibration and preliminary testing of a robotic telemanipulator for OCT guided retinal surgery, in *IEEE Int. Conf. Robot. Autom.*, (2013), pp. 225–231.
29. L. A. Lyons, R. J. Webster III and R. Alterovitz, Motion Planning for Active Cannulas, in *Proc. IEEE/RSJ Int. Conf. Intell. Robot. Syst. (IROS)*, October (2009), pp. 801–806.
30. E. J. Butler, R. Hammond-Oakley, S. Chawarski, A. H. Gosline, P. Codd, T. Anor, J. R. Madsen, P. E. Dupont and J. Lock, Robotic neuro-endoscope with concentric tube augmentation, in *IEEE/RSJ Int. Conf. Intelligent Robots and Systems* (2012), pp. 2941–2946.
31. P. J. Swaney, J. M. Croom, J. Burgner, H. B. Gilbert, D. C. Rucker, P. T. Russell III, K. D. Weaver and R. J. Webster III, Design of a quadramanual robot for single-nostril skull base surgery, *ASME Dyn. Syst. Control Conference* (2012).
32. R. J. Webster III, J. S. Kim, N. J. Cowan, G. S. Chirikjian and A. M. Okamura, Nonholonomic modeling of needle steering, in *The Int. J. Robot. Res.* **25**(5–6) (2006) 509–525.
33. N. Abolhassani, R. V. Patel and M. Moallem, Needle insertion into soft tissue: A survey, *Med. Eng. Phys.* **29**(4) (2007) 413–431.
34. K. B. Reed, A. Majewicz, V. Kallem, R. Alterovitz, K. Goldberg, N. J. Cowan and A. M. Okamura, Robot-assisted needle steering, *IEEE Robot. Autom. Magaz.* **18**(4) (2011) 35–46.
35. P. J. Swaney, J. Burgner, H. B. Gilbert and R. J. Webster III, A flexure-based steerable needle: High curvature with reduced tissue damage, *IEEE Trans. Biomed. Eng.* **60** (2013) 906–909.
36. L. A. Lyons, R. J. Webster III and R. Alterovitz, Planning active cannula configurations through tubular anatomy, in *IEEE Int. Conf. Robotics and Automation* (2010), pp. 2082–2087.
37. L. G. Torres, R. J. Webster III, and R. Alterovitz, Task-oriented design of concentric tube robots using mechanics-based models, in *IEEE/RSJ Int. Conf. Intelligent Robots and Systems* (2012), pp. 4449–4455.
38. D. C. Rucker, J. Das, H. B. Gilbert, P. J. Swaney, M. I. Miga, N. Sarkar and R. J. Webster III, Sliding mode control of steerable needles, *IEEE Trans. Robot.* **29** (2013) 1289–1299.
39. E. P. Lamers, A. A. Remirez, P. J. Swaney and R. J. Webster III, A bronchial puncture mechanism for transoral access to the lung parenchyma, in *Design Medical Devices Conference* (2015).
40. P. J. Swaney, A. W. Mahoney, A. A. Remirez, E. P. Lamers, B. I. Hartley, R. H. Feins, R. Alterovitz and R. J. Webster III, Tendons, concentric tubes, and a bevel tip: Three steerable robots in one transoral lung access system, in *IEEE Int. Conf. Robotics and Automation* (2015), pp. 5378–5383.
41. D. Minhas, J. Engh and C. Riviere, Testing of neurosurgical needle steering via duty-cycled spinning in brain tissue *in vitro*, in *Int. Conf. IEEE Engineering in Medicine and Biology Society* (2009), pp. 258–261.
42. A. Majewicz, S. Marra, M. van Vledder, M. Lin, M. Choti, D. Song and A. Okamura, Behavior of tip-steerable needles in *ex vivo* and *in vivo* tissue, *IEEE Trans. Biomed. Eng.* **59**(10) (2012) 2705–2715.
43. R. J. Webster III and B. A. Jones, Design and kinematic modeling of constant curvature continuum robots: A review, *Int. J. Robot. Res.* **29**(13) (2010) 1661–1683.
44. R. J. Hendrick, C. R. Mitchell, S. D. Herrell and R. J. Webster III, Hand-held transendoscopic robotic manipulators: A transurethral laser prostate surgery case study, *Int. J. Robot. Res.* (Special Issue ISER2014) (in press).
45. H. B. Gilbert, J. Neimat and R. J. Webster III, Concentric tube robots as steerable needles: Achieving follow-the-leader deployment, *IEEE Trans. Robot.* **31**(2) (2015) 246–258.
46. P. J. Swaney, H. B. Gilbert, R. J. Hendrick, O. Commichau, R. Alterovitz and R. J. Webster III, Transoral steerable needles in the lung:

How non-annular concentric tube robots can improve targeting, *Hamlyn Symp. Medical Robotics* (2015).
47. J. Burgner-Kahrs, Task-specific design of tubular continuum robots for surgical applications, *Soft Robotics* (Springer, 2015), pp. 222–230.
48. C. Bergeles, A. H. Gosline, N. V. Vasilyev, P. J. Codd, P. J. del Nido and P. E. Dupont, Concentric tube robot design and optimization based on task and anatomical constraints, *IEEE Trans. Robotics* **31**(1) (2015) 67–84.
49. C. Baykal, L. G. Torres and R. Alterovitz, Optimizing design parameters for sets of concentric tube robots using sampling-based motion planning, in *IEEE/RSJ Int. Conf. Intelligent Robots and Systems* (2015), pp. 4381–4387.
50. V. A. Moyer, Screening for lung cancer: U.S. preventive services task force recommendation statement, *Ann. Int. Med.* **160**(5) (2014) 330–338.

Philip J. Swaney received his B.S. degree in mechanical engineering from The Pennsylvania State University, State College, PA, USA, in 2010. He then graduated in 2016 with a Ph.D. in Mechanical Engineering from Vanderbilt University, Nashville, TN, USA, where he was actively involved in the design of needle-sized surgical robots and tools for the treatment of diseases in the lung and brain. He was also the recipient of an NSF Graduate Research Fellowship in 2012.

Arthur W. Mahoney received his B.S. degree in Computer Science from Utah State University, Logan, UT, USA, in 2009, and his Ph.D. degree in Computing from the University of Utah, Salt Lake City, UT, USA, in 2014. He was a recipient of both an NSF IGERT Traineeship and an NSF Graduate Research Fellowship. He received the Best Poster Award at the 2013 Hamlyn Symposium on Medical Robotics. He is currently a postdoctoral researcher at Vanderbilt University, Nashville, TN, USA.

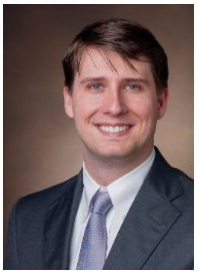

Bryan I. Hartley received his MD from Vanderbilt University Medical Center, Nashville, TN, USA and stayed at Vanderbilt for his diagnostic radiology residency. He recently finished a fellowship in vascular and interventional radiology and is now a Clinical Instructor in IR at Vanderbilt. Bryan's research interest is in minimally invasive medical device development to improve patient care.

Andria A. Remirez received her B.S. degree in Mechanical Engineering from Rice University, Houston, TX, USA, in 2013, and is currently a graduate student in Mechanical Engineering at Vanderbilt University. Her research focuses on the design, modeling and control of continuum robots and devices for surgical applications.

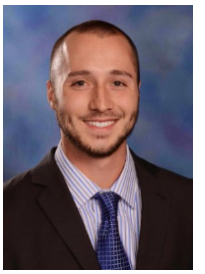

Erik Lamers received his B.S. degree in Mechanical Engineering from the University of Dayton, Dayton, OH, USA, in 2015. He is currently pursuing a Ph.D. degree in Mechanical Engineering at Vanderbilt University where he is a graduate research assistant in the Biomechanics and Assistive Technology Lab.

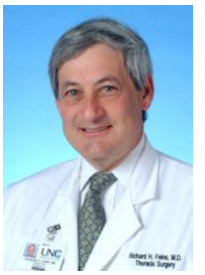

Richard H. Feins received his MD degree from the University of Vermont and his training in general surgery and cardiothoracic surgery at the University of Rochester. He was the chief of General Thoracic Surgery at the University of Rochester from 1988 until 2005 and at the University of North Carolina at Chapel Hill from 2005 until 2011. He initiated the navigational bronchoscopy program at UNC in 2006 and has been actively involved with the diagnosis and treatment of lung cancer for over 30 years. Dr. Feins was the principle investigator of a 3 year, multi-center study of simulation based training as a pathway to safer surgery. He presently is a Professor of Surgery in the Division of Cardiothoracic Surgery at UNC and is the Medical Director of Perioperative Services at UNC Hospitals.

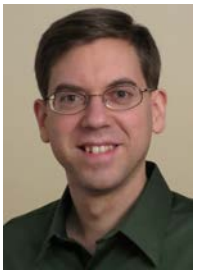

Ron Alterovitz Ron Alterovitz received a B.S. degree with Honors from Caltech, Pasadena, CA, USA in 2001 and a Ph.D. degree in industrial engineering and operations research at the University of California, Berkeley, CA, USA in 2006. He is currently an Associate Professor in the Department of Computer Science at the University of North Carolina at Chapel Hill, NC, USA, where he leads the Computational Robotics Research Group. His research focuses on motion planning for medical and assistive robots. Prof. Alterovitz has co-authored a book on Motion Planning in Medicine, was co-awarded a patent for a medical device, and has received multiple best paper finalist awards at IEEE robotics and computer-assisted medicine conferences. He is the recipient of an NIH Ruth L. Kirschstein National Research Service Award, two UNC Computer Science Department Excellence in Teaching Awards, and an NSF Early Career Development (CAREER) Award.

Robert J. Webster III received the B.S. degree in electrical engineering from Clemson University, Clemson, SC, USA, in 2002, and the M.S. and Ph.D. degrees in mechanical engineering from The Johns Hopkins University, Baltimore, MD, USA, in 2004 and 2007, respectively. In 2008, he joined the Faculty of Vanderbilt University. He is currently an Associate Professor of Mechanical Engineering, Electrical Engineering, Otolaryngology, Neurological Surgery, and Urologic Surgery, and directs the Medical Engineering and Discovery Laboratory. He serves on the steering committee for the Vanderbilt Institute in Surgery and Engineering, which brings together physicians and engineers to solve challenging clinical problems. He is the Chair of the SPIE Image-Guided Procedures, Robotic Interventions, and Modeling Conference, and is an Associate Editor for IEEE Transactions on Robotics. His research interests include surgical robotics, image-guided surgery, and continuum robotics. Dr. Webster received the IEEE Robotics & Automation Society Early Career Award, the National Science Foundation CAREER award, the Robotics Science and Systems Early Career Spotlight Award, and the IEEE Volz Award.